TRI-PP-90-27
June 1990

A relativistic, meson exchange model of pion-nucleon scattering

B.C. Pearce and B.K. Jennings
TRIUMF, 4004 Wesbrook Mall, Vancouver, B.C., Canada V6T 2A3

A relativistic meson exchange approach to the pion-nucleon interaction is developed using a three dimensional relativistic two body propagator and the results using different propagators compared. The relativistic approach is able to describe low energy scattering up to 400 MeV above threshold, while preserving the soft pion theorems. The different propagators give similar results, as the form factors necessary to get a fit suppress much of the multiple scattering.

(Submitted to Nuclear Physics A)

1. Introduction

The Dirac equation and two body generalizations have been used extensively for nucleon-nucleon[1,2] and nucleon-nucleus (see for example ref. [3]) scattering. However in the pion-nucleus problems the nucleons are almost invariably treated non-relativistically[4,5]. This lack of compatibility has lead to problems in describing processes such as proton induced pion production[6] which involve both pions and nucleons interacting with a nuclear medium. It is also expected that a relativistic approach would be useful for processes such as pion photo-production. In this paper we report the results of a fit to the πN phase shifts with a model utilizing a phenomenological meson-baryon Lagrangian and the smooth, relativistic, two-body propagator of ref. [7]. We restrict our considerations to pion kinetic energies below 400 MeV since at higher energies, resonances beyond the Δ and the coupling to the $\pi\Delta$ channel, which we have not included, become important. We also present a comparison of the results obtained using that smooth propagator, the Blankenbecler-Sugar propagator[8,9] and a K-matrix approach. We provide a complete description of the model and discuss the relative importance of the various terms in the Lagrangian. The crucial role of the form-factors is also discussed.

The model uses the nucleon, crossed nucleon, Δ, crossed Δ and ρ and σ exchange as driving terms in a three-dimensional reduction of the Bethe-Salpeter equation. Once we have specified the Lagrangian, an exact solution could in principle be obtained by solving the Bethe-Salpeter equation, with a "potential" consisting of all diagrams that do not have an intermediate state with exactly two particle lines. Of course, in practice this is impossible to do and it is usual to approximate the two-particle propagator and truncate the potential. However, this leads to problems if there is a large degree of cancellation between diagrams that are retained by solving the integral equation and diagrams that are omitted by truncating the potential. In particular, symmetries present in the Lagrangian may be violated in the solution to the integral equation. In the case of the πN system, problems arise in the S-waves if the chiral symmetry of the Lagrangian is destroyed by including some higher order diagrams via the solution of an integral equation but not including in the potential, diagrams that tend to cancel them[10]. In the original derivation of the smooth propagator[7] an attempt was made to address this problem by eliminating all short-range behavior from the two-body propagator. Hence, if the potential is to be truncated (as it must) it may be better to use an approximate two-body propagator that restores chiral symmetry (i.e. the smooth propagator) than to solve the Bethe-Salpeter equation. In the present case it turns out that in order to get a fit, the form factors must be sufficiently soft that the multiple scattering plays a relatively small role.

In sect. 2 the model is described in considerable detail including the Lagrangian, the integral equation and the method of solving it, the form factors and the renormalization procedure. In sect. 3 we present the results of a fit to the Karlsruhe[11] phase shifts. We also present a comparison of three propagators, demonstrate the relative importance of the various driving terms and discuss the soft pion theorems. Our conclusions are presented in sect. 4.

2. Description of the model

2.1. *The integral equation*

The starting point is the Bethe-Salpeter equation, which can be written using Jacobi coordinates as

$$\mathcal{T}(p,p';s) = \mathcal{V}(p,p';s) + \int \frac{d^4p''}{(2\pi)^4}\,\mathcal{V}(p,p'';s)\mathcal{G}_{BS}(p'';s)\mathcal{T}(p'',p';s). \tag{1}$$

Here the Bethe-Salpeter propagator, $\mathcal{G}_{BS}$, is just the product of Feynman propagators for the intermediate pion and nucleon. The Jacobi coordinates[12] are related to the pion and nucleon four-momenta p_π and p_N by

$$P = p_\pi + p_N; \qquad p = \frac{\varepsilon_\pi(s)p_N - \varepsilon_N(s)p_\pi}{\varepsilon_N(s) + \varepsilon_\pi(s)}, \tag{2}$$

where

$$\varepsilon_N(s) = \frac{s + m_N^2 - m_\pi^2}{2\sqrt{s}}; \qquad \varepsilon_\pi(s) = \frac{s + m_\pi^2 - m_N^2}{2\sqrt{s}}. \tag{3}$$

Also, s is the usual Mandelstam parameter, $s = P^2$. We always work in the centre-of-mass frame where $P = (\sqrt{s}, \underset{\sim}{0})$ and all the propagators we consider contain the factor $\delta(p \cdot P)$. In this case, the inverse relations are simply

$$p_N = (\varepsilon_N(s), \underset{\sim}{p}); \qquad p_\pi = (\varepsilon_\pi(s), -\underset{\sim}{p}) \tag{4}$$

We will use the notation p to refer to the magnitude of the three-momentum $\underset{\sim}{p}$ and $\hat{p}$ for the unit vector in the direction of $\underset{\sim}{p}$.

There are an infinite number of ways of reducing the four-dimensional integral in Eq. (1) to three dimensions while retaining the two-body unitarity cut. We shall consider three different forms. The smooth propagator[7,9] replaces $\mathcal{G}_{BS}$ in Eq (1) with

$$\mathcal{G}_{sm}(p;s) = 2\pi\frac{\delta(p_0)}{2\sqrt{s}}\,\frac{\gamma_0\varepsilon_N(s) - \underset{\sim}{\gamma}\cdot\underset{\sim}{p} + m_N}{\varepsilon_N^2(s) - m_N^2 - \mathrm{p}^2}. \tag{5}$$

This propagator has had all short-range structure explicitly removed.

The Blankenbecler-Sugar[8,9] propagator is

$$\mathcal{G}_{BbS}(p;s) = 2\pi\frac{\delta(p_0)}{2\sqrt{s}}\left(\sqrt{\frac{s_p}{s}}\,\frac{ss_p - (m_N^2 - m_\pi^2)^2}{s_p^2 - (m_N^2 - m_\pi^2)^2}\right)\frac{\gamma_0\sqrt{\mathrm{p}^2 + m_N^2} - \underset{\sim}{\gamma}\cdot\underset{\sim}{p} + m_N}{\varepsilon_N^2(s) - m_N^2 - \mathrm{p}^2}, \tag{6}$$

where

$$s_p = \left(\sqrt{\mathrm{p}^2 + m_N^2} + \sqrt{\mathrm{p}^2 + m_\pi^2}\right)^2. \tag{7}$$

This is simpler to work with since it is proportional to a positive energy projection operator. However it does not have the correct limit as either particle becomes infinitely heavy (the

one-body limit). While this is probably satisfactory in an equal-mass system such as nucleon-nucleon, it may become a problem for the pion-nucleon system.

The simplest propagator of all is the K-matrix which simply discards all contributions to the principal value part of the integral. For completeness, it can be written in the same form as the other two as

$$\mathcal{G}_K(p;s) = -2i\pi^2 \frac{\delta(p_0)}{2\sqrt{s}}(\not{p}_N + m_N)\delta(p_N^2 - m_N^2). \tag{8}$$

Performing a partial wave expansion of the integral equation is considerably more difficult with the smooth propagator since there is no projection operator onto positive energy states present. The method used is described in detail in ref. [13]. We sketch the main points here for completeness.

To perform the partial wave expansion, define a 4×2 matrix $\mathcal{Y}$ by

$$\mathcal{Y}^l_{JM_J}(\hat{p}) = \begin{pmatrix} \phi^l_{JM_J}(\hat{p}) & 0 \\ 0 & \underline{\sigma}\cdot\hat{p}\,\phi^l_{JM_J}(\hat{p}) \end{pmatrix}, \tag{9}$$

where ϕ results from coupling a two component spinor, χ_m, to orbital angular momentum l,

$$\phi^l_{JM_J}(\hat{p}) = \sum_{m,m_l} (\tfrac{1}{2} m l m_l | JM_J) Y_{lm_l}(\hat{p})\chi_m. \tag{10}$$

The $\mathcal{Y}^l_{JM_J}$ matrices are eigenstates of J^2, J_z and parity. They also are orthogonal and complete in the sense that

$$\int d\hat{p}\, \mathcal{Y}^{l\dagger}_{JM_J}(\hat{p})\mathcal{Y}^{l'}_{J'M'_J}(\hat{p}) = \delta_{ll'}\delta_{JJ'}\delta_{M_JM'_J} I_2, \tag{11}$$

and

$$\sum_{lJM_J} \mathcal{Y}^l_{JM_J}(\hat{p})\mathcal{Y}^{l\dagger}_{JM_J}(\hat{p}') = \delta(\hat{p}-\hat{p}')I_4, \tag{12}$$

where I_2 and I_4 are the 2 and 4 dimensional unit matrices respectively. Any $\pi N \to \pi N$ Feynman amplitude $\mathcal{V}(p,p';s)$ (a 4×4 matrix) can be written as

$$\mathcal{V}(p,p';s) = \sum_{lJM_J} \mathcal{Y}^l_{JM_J}(\hat{p})\hat{V}^{lJ}(p_0,\mathrm{p};p'_0,\mathrm{p}';s)\mathcal{Y}^{l\dagger}_{JM_J}(\hat{p}') \tag{13}$$

with

$$\hat{V}^{lJ}(p_0,\mathrm{p};p'_0,\mathrm{p}';s) = \int d\hat{p}\, d\hat{p}'\, \mathcal{Y}^{l\dagger}_{JM_J}(\hat{p})\mathcal{V}(p,p';s)\mathcal{Y}^l_{JM_J}(\hat{p}'), \tag{14}$$

Throughout, we use the notation $\mathcal{V}$, $\mathcal{T}$, $\mathcal{G}$ to refer to 4×4 matrices, $\hat{V}$ etc. for 2×2 matrices and V for ordinary numbers. It is now a simple matter to use these relations to perform a partial wave expansion of the Bethe-Salpeter equation (Eq. (1)). Using $\mathcal{G}_{sm}$ in place of $\mathcal{G}_{BS}$ (which sets $p_0 = 0$ so we drop p_0 from the argument list of $\hat{V}$), we obtain a one-dimensional integral equation for the 2×2 matrix $\hat{T}$

$$\begin{aligned} \hat{T}^{lJ}(\mathrm{p},\mathrm{p}';s) &= \hat{V}^{lJ}(\mathrm{p},\mathrm{p}';s) \\ &+ \int_0^\infty d\mathrm{p}''\,\mathrm{p}''^2 \hat{V}^{lJ}(\mathrm{p},\mathrm{p}'';s)\hat{G}_{sm}(\mathrm{p}'';s)\hat{T}^{lJ}(\mathrm{p}'',\mathrm{p}';s), \end{aligned} \tag{15}$$

where

$$\hat{G}_{sm}(\mathrm{p};s) = \frac{1}{(2\pi)^3}\frac{1}{2\sqrt{s}}\frac{1}{\varepsilon_N^2(s) - m_N^2 - \mathrm{p}^2}\begin{pmatrix} \varepsilon_N(s)+m_N & -\mathrm{p} \\ \mathrm{p} & -\varepsilon_N(s)+m_N \end{pmatrix}. \tag{16}$$

The partial wave matrix $\hat{T}^{lJ}$ is related to the usual partial wave T-matrix, T^{lJ}, via

$$T^{lJ}(\mathrm{p},\mathrm{p}';s) = \overline{u}(\mathrm{p};s)\hat{T}^{lJ}(\mathrm{p},\mathrm{p}';s)u(\mathrm{p}';s), \tag{17}$$

where

$$u(\mathrm{p};s) = \sqrt{\frac{\varepsilon_N(s)+m_N}{2m_N}}\begin{pmatrix} 1 \\ \dfrac{\mathrm{p}}{\varepsilon_N(s)+m_N} \end{pmatrix}, \tag{18}$$

$$\overline{u}(\mathrm{p};s) = u^\dagger(\mathrm{p};s)\sigma_z, \tag{19}$$

with a similar expression for the potential. Expressions for the $\hat{V}^{lJ}$ are given in the appendix. In the above, we have suppressed the isospin indices.

The method outlined here is equivalent to using the identity operator, expressed as the sum of projection operators onto positive and negative states, to generate a set of coupled equations between $\overline{u}\mathcal{T}u$, $\overline{u}\mathcal{T}v$, $\overline{v}\mathcal{T}u$, and $\overline{v}\mathcal{T}v$. However, the method used here has the (mainly aesthetic) advantage of paralleling closely the usual non-relativistic expansion.

2.2. *The Lagrangian*

The interaction Lagrangian is

$$\begin{aligned}\mathcal{L} &= \frac{g_{\pi NN}}{2m_N}\overline{\psi}_N\gamma_5\gamma^\mu\underset{\sim}{\tau}\cdot\partial_\mu\underset{\sim}{\pi}\psi_N + \frac{g_{\pi N\Delta}}{m_\pi}\overline{\psi}^\mu_\Delta(g_{\mu\nu}+x_\Delta\gamma_\mu\gamma_\nu)\underset{\sim}{T}\cdot\partial^\nu\underset{\sim}{\pi}\psi_N \\ &+ g_\rho\overline{\psi}_N\tfrac{1}{2}\underset{\sim}{\tau}\cdot(\gamma^\mu\underset{\sim}{\rho}_\mu + \frac{\kappa_\rho}{2m_N}\sigma^{\mu\nu}\partial_\nu\underset{\sim}{\rho}_\nu)\psi_N + g_\rho\underset{\sim}{\rho}^\mu\cdot\underset{\sim}{\pi}\times\partial_\mu\underset{\sim}{\pi} \\ &+ g_{\sigma NN}\overline{\psi}_N\sigma\psi_N + \frac{g_{\sigma\pi\pi}}{2m_\pi}\sigma\partial_\mu\underset{\sim}{\pi}\cdot\partial^\mu\underset{\sim}{\pi}.\end{aligned} \tag{20}$$

Since we are only sensitive to the product $g_{\rho NN}g_{\rho\pi\pi}$, we can assume universality ($g_{\rho NN} = g_{\rho\pi\pi} = g_\rho$). Both vector and tensor couplings of the ρ meson to the nucleon are used, however the tensor coupling comes out smaller than normally obtained. The $\sigma\pi\pi$ vertex is chosen to be chirally symmetric which implies a derivative coupling to the pion.

The Δ is treated relativistically as a Rarita-Schwinger particle. The parameter x_Δ controls the second form of the $\pi N\Delta$ vertex which arises when the Δ is treated relativistically. There is an ambiguity whether this degree of freedom is put into the propagator or into the vertex[14]. We put the freedom in the vertex, taking the Δ propagator, S, from Eq. (10) of ref. [14] with $A = -1$, i.e.

$$S_{\mu\nu}(p) = \frac{\not{p}+m_\Delta}{p^2-{m_\Delta}^2}\left[-g_{\mu\nu}+\frac{1}{3}\gamma_\mu\gamma_\nu+\frac{2}{3m_\Delta^2}p_\mu p_\nu - \frac{1}{3m_\Delta}(p_\mu\gamma_\nu-\gamma_\mu p_\nu)\right] \tag{21}$$

From this Lagrangian we construct the six potentials corresponding to the diagrams shown in fig. 1 (i.e., s- and u-channel nucleon and delta exchange, and t-channel rho and sigma exchange) by inserting the Feynman amplitude for each process into Eq. (14). Explicit forms are given in Appendix A.

2.3. *Form factors*

A consequence of the derivative couplings in the Lagrangian is that the form factors must depend on more than just t (see ref. [2]) as is usually done in the meson exchange NN potentials. For example, if only the t-dependent form-factor, $f_\sigma^2(t)$ were kept in the σ-exchange diagram (Eq. (A25)) then we find $\hat{V}_\sigma^{IJT}$ diverges as $\mathrm{p} \to \infty$. The solution is to make the form factors functions of the squares of the momenta of each leg. For a vertex with legs α, β, γ and four-momenta p_α, p_β, p_γ the form factor we use is

$$f_{\alpha\beta\gamma}(p_\alpha^2, p_\beta^2, p_\gamma^2) = f_\alpha(p_\alpha^2) f_\beta(p_\beta^2) f_\gamma(p_\gamma^2) \tag{22}$$

with

$$f_\alpha(p^2) = \left(\frac{n_\alpha \Lambda_\alpha^4}{n_\alpha \Lambda_\alpha^4 + (p^2 - m_\alpha^2)^2} \right)^{n_\alpha}. \tag{23}$$

The function f_α is constructed to have a maximum value ($= 1$) when the leg is on-mass-shell. For large n_α, f_α approaches a Gaussian in $(p^2 - m_\alpha^2)$ with width Λ_α^2.

With this form, the combination of form factors associated with each off-shell Born term is a function of five of the six possible linearly independent scalars. When iterated using a propagator of the form of Eq. (5), the delta function in p_0 (which generalizes to $\delta(p \cdot P)$ in an arbitrary frame) adds two conditions, one each to the initial and final state variables, making the combined form factor a function of three independent variables. If all external legs are on-shell, it reduces to a function of only one of s, t or u, depending on the exchange type.

It is interesting to compare the πNN form-factor defined this way with that used by other authors. By πNN form factor, we mean the vertex function that appears in the nucleon pole diagram. In our case this is a function of s and p,

$$f_{\pi NN}(\mathrm{p}, s) = f_N(\varepsilon_N^2(s) - \mathrm{p}^2) f_\pi(\varepsilon_\pi^2(s) - \mathrm{p}^2) f_N(s). \tag{24}$$

In fig. 2a we show the p dependence of our form-factor with $\sqrt{s} = m_N$ (solid curve), the cloudy bag model[15] with $R = 1.0$ fm (dashed curve) and the monopole form factor of the Bonn potential with a cutoff parameter of 1300 MeV[16] (dash-dotted curve). Figure 2b shows the s dependence of our πNN form factor. The solid curve is for $\sqrt{s} = m_N$, the dashed curve is at threshold where $\sqrt{s} = m_N + m_\pi$, and the dash-dotted curve is with $\sqrt{s} = 1400$ MeV.

2.4. *Renormalization*

Since solving the integral equation renormalizes the nucleon and Δ couplings and masses, we use bare values for the masses (m_{0N} and $m_{0\Delta}$) and couplings ($g_{0\pi NN}$ and $g_{0\pi N\Delta}$)

of the pole diagrams in the P_{11} and P_{33} channels. The bare nucleon parameters are calculated by the renormalization procedure[17] and hence are not free parameters but functions of the other parameters. The renormalization is driven by the requirements that the P_{11} amplitude have a pole at the physical nucleon mass and that the residue reproduce the physical πNN coupling constant. In principle, $m_{0\Delta}$ and $g_{0\pi N\Delta}$ could be determined by the same procedure but we treat them as parameters to avoid having to solve an integral equation for complex energy. Since these are tightly constrained by the P_{33} resonance, they can essentially be regarded as functions of the other parameters also.

3. Results

The results of a fit to the S- and P-wave Karlsruhe phase shifts[11] using the smooth propagator are presented in the solid curves of fig. 3. The corresponding parameters are those from the first column in Table 1 (i.e. the "Smooth" parameters). The scattering lengths and volumes are presented in the first column of Table 2. It can be seen that we get a good fit to the phase shift analysis, even in the S-waves which traditionally cause trouble. This is achieved by paying careful attention to chiral symmetry rather than by the ad hoc addition of short range repulsion. The scattering lengths are reproduced to 20%.

In Table 3 we also make a comparison between the parameters from this fit and those of other authors. When comparing g_ρ one must be wary of the effect of the form factor. With our form factors, the coupling constant defines the strength at the t-channel pole ($t = m_\rho^2$) but the contribution to the scattering lengths comes from $t = 0$. Hence, in Table 3 we also indicate the value of g_ρ at $t = 0$. The values of the coupling constants are in good agreement with those from other sources except for the tensor ρNN coupling (κ_ρ) which is considerably too low. It should be noted that Höhler and Pietarinen[18], who find $\kappa_\rho = 6.6$, have different form factors for the vector and tensor ρNN couplings. A consequence of this is that κ_ρ is a function of t. The quoted value of $\kappa_\rho = 6.6$ corresponds to $t = m_\rho^2$ but at $t = 0$, they have $\kappa_\rho = 3.7$. It is worth remembering that, in the scattering region, the ρNN vertex only enters with $-\infty < t < 0$.

The sigma mass and cut off parameters are comparable, but, since the sigma exchange should be regarded as a means of mocking up correlated two-pion exchanges rather than a real meson exchange, this is not a major concern. A fit was also tried allowing for a non-chirally-symmetric $\sigma\pi\pi$ coupling, $\sigma\underset{\sim}{\pi}\cdot\underset{\sim}{\pi}$, in addition to the chirally-symmetric version but this did not improve the fit significantly.

The large value of $n_\alpha = 10$ that we have used in the form factors means that our form factors are essentially Gaussians. However this arbitrary choice is not crucial to the fits. A fit of equal quality can be obtained with $n_\alpha = 1$. Large values for n_α have the numerical advantage of pushing the poles in the integration variable p'' arising from the form factors, further from the real p'' axis.

The crucial ingredient in getting the correct low energy behavior in the P_{11} partial wave seems to be the renormalization of the nucleon (as was also observed in refs. [17] and [19]). It is well known that the sign change comes about due to a cancellation between

the repulsion from the nucleon pole and the attractive non-pole contribution from the other diagrams. By requiring that the amplitude have a pole at the physical nucleon mass with the correct residue, we completely specify the balance between the pole and non-pole contributions. Thus even when we excluded the P_{11} partial wave from the least-squares minimization process a quite reasonable fit to the P_{11} partial wave was obtained since we always apply the renormalization procedure. This can be viewed as an illustration of the importance of crossing symmetry to the P_{11} partial wave. Diagrams summed by solving the integral equation have a significant effect on the position and residue of the s-channel pole. However, the u-channel pole from the crossed nucleon diagram is unaffected. The renormalization is crucial to get the cancellation between these poles which is, in turn, necessary to obtain the small P_{11} phase shifts.

3.1. *Comparison of three propagators*

There are two ways we can compare the three propagators presented in sect. 2. First, in fig. 3 we compare the phase shifts obtained using the same parameter set with each of the three propagators. The solid curve is the fit obtained using the smooth propagator, the dashed curve is with the Blankenbecler-Sugar propagator of Eq. (6) while the dash-dotted curve uses the K-matrix. For the Blankenbecler-Sugar propagator, the bare nucleon parameters ($g_{0\pi NN}$ and m_{0N}) were set as described above and the bare delta parameters ($g_{0\pi N\Delta}$ and $m_{0\Delta}$) were adjusted to fit the P_{33} channel. Since the K-matrix propagator produces no renormalization of the nucleon and delta poles, the bare parameters were set to the physical values in this case. All other parameters were kept the same for this comparison. A table of the bare parameters used in producing fig. 3 is given in table 4.

The second comparison is to refit the parameters to the phase shift analysis for the Blankenbecler-Sugar and K-matrix propagators. This comparison is shown in fig. 4. Again, the solid curve is the fit using the smooth propagator, the dashed curve is with the Blankenbecler-Sugar propagator and the dash-dotted curve is the K-matrix fit. The parameters can be found in table 1. The scattering lengths from these fits are listed in table 2.

It is evident from this comparison that the effect of multiple scattering on the S, P_{13} and P_{31} partial waves in our model is small. The effect in the P_{11} and P_{33} channels is mostly to simply renormalize the bare masses and coupling constants (see tables 4 and 1). Overall, the inclusion of multiple scattering improves the fit slightly. The size of the multiple scattering effect is largely controlled by the parameter Λ_π (actually by the smaller of Λ_π and Λ_N). This is because the product $f_\pi^2(p_\pi^2)f_N^2(p_N^2)$ appears in every πN intermediate state. If left completely free, a slightly better fit was obtained with $\Lambda_\pi \approx 300$ MeV. With such a small cutoff, the multiple scattering was effectively killed, the improvement to the P_{31} partial wave being the main thing preventing Λ_π from running all the way down to zero. In the fits presented here, Λ_π was constrained to be greater than 700 MeV, but since the fit would prefer a lower value, this amounted to fixing Λ_π at this value. If Λ_π is increased the fit tends to deteriorate. Also, the renormalization of the bare nucleon and delta becomes large.

3.2. *The Born Contributions*

It is instructive to examine the relative contributions that each of the six diagrams of fig. 1 have to the total amplitude. In fig. 5 we show the contributions for each partial wave resulting from the fit using the smooth propagator (the solid curves of figs. 3 and 4). The quantity plotted is the usual partial wave potential, $V^{IJT}(\mathrm{k},\mathrm{k};s)$ (see Eq. (17)) where k is the on-shell momentum obtained from the pole position of Eq. (16). In these figures, the letter beside the curve refers to which diagram from fig. 1 the curve corresponds. The pole contributions are omitted from the P_{11} and P_{33} plots to show more clearly the effects of the other diagrams.

One remarkable thing about these curves is the large contribution made by the Nucleon pole to the S_{11} channel and the Delta pole to the S_{31} channel. These contributions would be absent from a non-relativistic analysis. They arise because the diagrams for s-channel poles include the time-ordered graph corresponding to an anti-particle intermediate state.

Also it is evident that the sigma exchange plays a rather minor role. In fact, omitting the sigma exchange merely results in a slight degradation in the fit to the S-waves in the $T_\pi = 20$–100 MeV range. Since the sigma exchange should be regarded as a means of mocking up higher order processes rather than the exchange of a real meson, this result is rather pleasing. It implies that the contribution from such processes is small as one would expect.

3.3. *The soft pion theorems*

A major success of the soft pion theorems is the Weinberg-Tomozawa relation for the scattering length for S-wave scattering of a pion from any target. In terms of the Lagrangian given in Eq. (20), the relation is equivalent to the statement that, in the soft pion limit, the scattering lengths are dominated by ρ-exchange. That is,

$$a_{S+} \equiv \tfrac{1}{3}(a_{S_{11}} + 2a_{S_{31}}) = O\left(\frac{m_\pi^2}{m_N^2}\right) \tag{25}$$

and

$$a_{S-} \equiv \tfrac{1}{3}(a_{S_{11}} - a_{S_{31}}) = \frac{g_\rho^2}{4\pi}\frac{f_\rho^2(0)}{m_\rho^2} m_\pi + O\left(\frac{m_\pi^2}{m_N^2}\right). \tag{26}$$

Frequently however, iterating the Born diagrams in a Lippmann-Schwinger equation destroys this property. In fig. 6a we illustrate that this feature is preserved in our calculation by plotting the S-wave scattering lengths as a function of the pion mass. (Note that the pion mass appears in the $\pi N\Delta$ and $\sigma\pi\pi$ couplings of Eq. (20) merely as scale parameter to keep the couplings dimensionless. Hence in these cases it was kept fixed at the physical value.) We see that a_{S-} is linear in m_π while a_{S+} is quadratic, in agreement with the soft pion theorems. Also, the slope of a_{S-} near $m_\pi = 0$ is within 1% of the value obtained using Eq. (26). This indicates that the iteration of the potential has not destroyed the soft pion theorems.

In fig. 6b we show a similar plot from the fit using the Blankenbecler-Sugar propagator. Again, a_{S^-} exhibits linear behavior with a slope consistent with the ρ-exchange potential. We found this result somewhat surprising since the smooth propagator was constructed to have this property but the Blankenbecler-Sugar was not. The secret would appear to lie in the fact that, in the form we have presented them, both propagators ensure that there is no energy transfer through the potentials. This is imposed by the factor $\delta(p_0)$ (or $\delta(p \cdot P)$ if the centre-of-mass frame is not used) which is common to both propagators. This means that the pion energy that enters in evaluating the potentials in intermediate states is the on-shell value, $\varepsilon_\pi(s)$ rather than $\sqrt{\mathbf{p}^2 + m_\pi^2}$, which would be obtained if the pion where kept on-mass-shell. With either the smooth or Blankenbecler-Sugar propagator and the present form factors, the effect of multiple scattering in the S-waves is small. This also aids in satisfying the Weinberg-Tomozawa relation since it is exactly satisfied in Born approximation.

4. Conclusions

We have presented a relativistic meson exchange potential that fits the pion-nucleon scattering data up to $T_\pi = 400$ MeV. Besides the value of this work in it own right, it can serve as a starting point for work in various other directions. For example it could be used to develop a pion-nucleus optical potentials or using SU(3) it could be extended to kaon and anti-kaon scattering.

To go beyond 400 MeV would require additional physics, namely the inclusion of higher resonances beyond the Δ (for example the Roper) and the coupling to the $\pi\Delta$ channel. The parameters from the current fit are consistent with the traditional values with the exception of the ρNN tensor coupling. This comes out rather small in our fit. However this may be due to the fact that we have not included separate form factors for the vector and tensor couplings.

The sigma meson is seen to have relatively little effect in any partial wave, which is reassuring since it is fictitious anyway. By way of contrast the rho meson is important in several partial waves. The remaining diagrams — the pole and crossed pole diagrams — are important in some partial waves but not in others.

The form factors we have used differ from conventional usage in that they depend on the square of the 4-momentum of each leg rather than just the momentum transfer. With the derivative coupling the multiple scattering does not converge when the form factors depended on just the momentum transfer. It was necessary to use form factors that significantly suppress the multiple scattering in order to obtain a fit. The form factor cutoffs are consistent with cloudy bag model estimates. This suppression means that the choice of two body propagator is not crucial and that soft pion theorems are maintained. All the propagators used had a delta function on the energy transfer and we suspect that this is important, especially in getting the low energy theorems.

Acknowledgment: The Natural Sciences and Engineering Research Council of Canada is thanked for financial support.

Appendix A. The partial wave potentials

The partial wave input to Eq. (15) is obtained by using the Feynman amplitudes corresponding to the diagrams shown in fig. 1, in Eq. (14). In this Appendix we present explicit expressions for these potentials, including the isospin decomposition. The potentials are variously labeled with either lJT representing orbital angular momentum l, total angular momentum J and total isospin T or with the usual spectroscopic notation. We use the definition

$$l_\pm = J \pm \tfrac{1}{2}. \tag{A1}$$

In the following, s, u and t are the usual Mandelstam variables

$$\begin{aligned} s &= (p_N + p_\pi)^2 = (p'_N + p'_\pi)^2, \\ u &= (p_N - p'_\pi)^2 = (p'_N - p_\pi)^2 = (\sqrt{s} - 2\varepsilon_\pi(s))^2 - \mathrm{p}^2 - \mathrm{p}'^2 - 2\mathrm{p}\mathrm{p}'x, \\ t &= (p_N - p'_N)^2 = (p_\pi - p'_\pi)^2 = -\mathrm{p}^2 - \mathrm{p}'^2 + 2\mathrm{p}\mathrm{p}'x, \end{aligned} \tag{A2}$$

where

$$x = \hat{\mathrm{p}} \cdot \hat{\mathrm{p}}'. \tag{A3}$$

For off-shell particles, s, u and t satisfy

$$s + u + t = p_N^2 + p_N'^2 + p_\pi^2 + p_\pi'^2. \tag{A4}$$

We will omit the s argument of $\varepsilon_N(s)$ and $\varepsilon_\pi(s)$ as a notational convenience. The nucleon s-channel pole is

$$\widehat{V}_N^{S_{11}}(\mathrm{p},\mathrm{p}';s) = 12\pi \left(\frac{g_{\pi NN}}{2m_N}\right)^2 \frac{f_N(p_N^2) f_\pi(p_\pi^2) f_N(p_N'^2) f_\pi(p_\pi'^2) f_N^2(s)}{\sqrt{s} + m_N} \begin{pmatrix} \varepsilon_\pi^2 & \varepsilon_\pi \mathrm{p}' \\ -\varepsilon_\pi \mathrm{p} & -\mathrm{p}\mathrm{p}' \end{pmatrix}, \tag{A5}$$

$$\widehat{V}_N^{P_{11}}(\mathrm{p},\mathrm{p}';s) = 12\pi \left(\frac{g_{0\pi NN}}{2m_N}\right)^2 \frac{f_N(p_N^2) f_\pi(p_\pi^2) f_N(p_N'^2) f_\pi(p_\pi'^2) f_N^2(s)}{\sqrt{s} - m_{0N}} \begin{pmatrix} \mathrm{p}\mathrm{p}' & \varepsilon_\pi \mathrm{p} \\ -\varepsilon_\pi \mathrm{p}' & -\varepsilon_\pi^2 \end{pmatrix}. \tag{A6}$$

The nucleon u-channel pole is

$$\begin{aligned} \widehat{V}_N^{l_\pm JT}(\mathrm{p},\mathrm{p}';s) = -12\pi \left(\frac{g_{\pi NN}}{2m_N}\right)^2 & \begin{Bmatrix} 1 & \frac{1}{2} & T \\ 1 & \frac{1}{2} & \frac{1}{2} \end{Bmatrix} f_N(p_N^2) f_\pi(p_\pi^2) f_N(p_N'^2) f_\pi(p_\pi'^2) \int_{-1}^{+1} dx \frac{f_N^2(u)}{u - m_N^2} \\ \times \Bigg[& \begin{pmatrix} \varepsilon_\pi(\varepsilon_\pi \xi_- - 2\varepsilon_\pi^2 + \mathrm{p}^2 + \mathrm{p}'^2) + 2\mathrm{p}\mathrm{p}'x\xi_+ & \mathrm{p}'(\varepsilon_\pi \xi_+ - \varepsilon_\pi^2 + \mathrm{p}^2) \\ -\mathrm{p}(\varepsilon_\pi \xi_+ - \varepsilon_\pi^2 + \mathrm{p}'^2) & \mathrm{p}\mathrm{p}'\xi_- \end{pmatrix} P_l(x) \\ + & \begin{pmatrix} -\mathrm{p}\mathrm{p}'\xi_+ & \mathrm{p}(\varepsilon_\pi \xi_- - \varepsilon_\pi^2 + \mathrm{p}'^2) \\ -\mathrm{p}'(\varepsilon_\pi \xi_- - \varepsilon_\pi^2 + \mathrm{p}^2) & -\varepsilon_\pi(\varepsilon_\pi \xi_+ - 2\varepsilon_\pi^2 + \mathrm{p}^2 + \mathrm{p}'^2) - 2\mathrm{p}\mathrm{p}'x\xi_- \end{pmatrix} P_{l\mp 1} \Bigg], \end{aligned} \tag{A7}$$

where we have used

$$\xi_\pm = \sqrt{s} \pm m_N. \tag{A8}$$

For the delta s-channel pole we have

$$\widehat{V}_{\Delta}^{S_{31}}(\mathrm{p},\mathrm{p}';s) = 4\pi\left(\frac{g_{\pi N\Delta}}{m_\pi}\right)^2 \frac{f_N(p_N^2)f_\pi(p_\pi^2)f_N(p_N'^2)f_\pi(p_\pi'^2)f_\Delta^2(s)}{3m_\Delta}$$
$$\times \left[\varepsilon_\pi \begin{pmatrix} 2\frac{\varepsilon_\pi}{m_\Delta}(\sqrt{s}+m_\Delta) & -\mathrm{p}' \\ \mathrm{p} & 0 \end{pmatrix} + 2x_\Delta \begin{pmatrix} \varepsilon_\pi^2\left(\frac{2\sqrt{s}}{m_\Delta}-d_-\right) & \varepsilon_\pi \mathrm{p}'\left(\frac{\sqrt{s}}{m_\Delta}-d_-\right) \\ -\varepsilon_\pi \mathrm{p}\left(\frac{\sqrt{s}}{m_\Delta}-d_-\right) & \mathrm{pp}' d_- \end{pmatrix}\right], \tag{A9}$$

$$\widehat{V}_{\Delta}^{P_{31}}(\mathrm{p},\mathrm{p}';s) = 4\pi\left(\frac{g_{\pi N\Delta}}{m_\pi}\right)^2 \frac{f_N(p_N^2)f_\pi(p_\pi^2)f_N(p_N'^2)f_\pi(p_\pi'^2)f_\Delta^2(s)}{3m_\Delta}$$
$$\times \left[\varepsilon_\pi \begin{pmatrix} 0 & \mathrm{p} \\ -\mathrm{p}' & -2\frac{\varepsilon_\pi}{m_\Delta}(\sqrt{s}-m_\Delta) \end{pmatrix} - 2x_\Delta \begin{pmatrix} -\mathrm{pp}' d_+ & -\varepsilon_\pi \mathrm{p}\left(\frac{\sqrt{s}}{m_\Delta}+d_+\right) \\ \varepsilon_\pi \mathrm{p}'\left(\frac{\sqrt{s}}{m_\Delta}+d_+\right) & \varepsilon_\pi^2\left(\frac{2\sqrt{s}}{m_\Delta}+d_+\right) \end{pmatrix}\right], \tag{A10}$$

$$\widehat{V}_{\Delta}^{P_{33}}(\mathrm{p},\mathrm{p}';s) = 4\pi\left(\frac{g_{\pi N\Delta}}{m_\pi}\right)^2 \frac{f_N(p_N^2)f_\pi(p_\pi^2)f_N(p_N'^2)f_\pi(p_\pi'^2)f_\Delta^2(s)}{3(\sqrt{s}-m_\Delta)} \begin{pmatrix} \mathrm{pp}' & 0 \\ 0 & 0 \end{pmatrix}, \tag{A11}$$

$$\widehat{V}_{\Delta}^{D_{33}}(\mathrm{p},\mathrm{p}';s) = -4\pi\left(\frac{g_{\pi N\Delta}}{m_\pi}\right)^2 \frac{f_N(p_N^2)f_\pi(p_\pi^2)f_N(p_N'^2)f_\pi(p_\pi'^2)f_\Delta^2(s)}{3(\sqrt{s}+m_\Delta)} \begin{pmatrix} 0 & 0 \\ 0 & \mathrm{pp}' \end{pmatrix}, \tag{A12}$$

with

$$d_\pm = 1 + 2x_\Delta \pm \frac{\sqrt{s}x_\Delta}{m_\Delta}. \tag{A13}$$

The Delta u-channel pole gives rise to a somewhat complicated expression

$$\widehat{V}_{X\Delta}^{I_\pm JT}(\mathrm{p},\mathrm{p}';s) = \frac{4\pi}{3}\left(\frac{g_{\pi N\Delta}}{m_\pi}\right)^2 \begin{Bmatrix} 1 & \frac{1}{2} & T \\ 1 & \frac{1}{2} & \frac{3}{2} \end{Bmatrix} f_N(p_N^2)f_\pi(p_\pi^2)f_N(p_N'^2)f_\pi(p_\pi'^2)\int_{-1}^{+1} dx f_\Delta^2(u)$$
$$\times \left[\frac{\hat{A}_1 P_l(x)+\hat{B}_1 P_{l\mp1}}{u-m_\Delta^2} + \frac{2x_\Delta}{m_\Delta}\left(\hat{A}_2 P_l(x)+\hat{B}_2 P_{l\mp1}\right)\right], \tag{A14}$$

where

$$\hat{A}_1 = \left\{ \begin{pmatrix} -2\left(-\frac{\theta\theta'}{m_\Delta^2}+\varepsilon_\pi^2\right)(\zeta+m_\Delta) & -\mathrm{p}'\left(\frac{2\theta\theta'}{m_\Delta^2}+\varepsilon_\pi a-\frac{\sqrt{s}\theta}{m_\Delta}-2\varepsilon_\pi^2\right) \\ \mathrm{p}\left(\frac{2\theta\theta'}{m_\Delta^2}+\varepsilon_\pi a-\frac{\sqrt{s}\theta'}{m_\Delta}-2\varepsilon_\pi^2\right) & \mathrm{pp}'(a-\sqrt{s}) \end{pmatrix} \right.$$
$$\left. + \mathrm{pp}' x \begin{pmatrix} \frac{(2\zeta+m_\Delta)a}{m_\Delta}-\sqrt{s} & -\frac{\mathrm{p}'(2a-\zeta)}{m_\Delta} \\ \frac{\mathrm{p}(2a-\zeta)}{m_\Delta} & \frac{2\mathrm{pp}'}{m_\Delta} \end{pmatrix} + \frac{2\mathrm{p}^2\mathrm{p}'^2x^2}{m_\Delta^2}\begin{pmatrix} \zeta & -\mathrm{p}' \\ \mathrm{p} & 0 \end{pmatrix}\right\}, \tag{A15}$$

$$\hat{B}_1 = \left\{ \begin{pmatrix} \mathrm{pp}'(a+\sqrt{s}) & \mathrm{p}\left(-\frac{2\theta\theta'}{m_\Delta^2}+\varepsilon_\pi a-\frac{\sqrt{s}\theta'}{m_\Delta}+2\varepsilon_\pi^2\right) \\ -\mathrm{p}'\left(-\frac{2\theta\theta'}{m_\Delta^2}+\varepsilon_\pi a-\frac{\sqrt{s}\theta}{m_\Delta}+2\varepsilon_\pi^2\right) & -2\left(\frac{\theta\theta'}{m_\Delta^2}-\varepsilon_\pi^2\right)(\zeta-m_\Delta) \end{pmatrix} \right.$$
$$\left. + \mathrm{pp}'x \begin{pmatrix} \frac{2\mathrm{pp}'}{m_\Delta} & -\frac{\mathrm{p}(2a+\zeta)}{m_\Delta} \\ \frac{\mathrm{p}'(2a+\zeta)}{m_\Delta} & -\frac{(2\zeta-m_\Delta)a}{m_\Delta}+\sqrt{s} \end{pmatrix} + \frac{2\mathrm{p}^2\mathrm{p}'^2x^2}{m_\Delta^2}\begin{pmatrix} 0 & -\mathrm{p} \\ \mathrm{p}' & -\zeta \end{pmatrix} \right\}, \quad \text{(A16)}$$

$$\hat{A}_2 = \left\{ \begin{pmatrix} \varepsilon_\pi\left(\frac{b(\theta+\theta')}{m_\Delta}+\frac{2\varepsilon_\pi^2 x_\Delta}{m_\Delta}-\varepsilon_\pi d_+\right) & -\frac{\mathrm{p}'}{m_\Delta}(\varepsilon_\pi(\varepsilon_\pi-m_\Delta c)-b(\theta+\varepsilon_\pi^2)) \\ \frac{\mathrm{p}}{m_\Delta}(\varepsilon_\pi(\varepsilon_\pi-m_\Delta c)-b(\theta'+\varepsilon_\pi^2)) & -\mathrm{pp}'d_- \end{pmatrix} \right.$$
$$\left. + \mathrm{pp}'x \begin{pmatrix} 2\left(d_+ + \frac{\varepsilon_\pi}{m_\Delta}\right) & \frac{\mathrm{p}'}{m_\Delta} \\ -\frac{\mathrm{p}}{m_\Delta} & 0 \end{pmatrix} \right\}, \quad \text{(A17)}$$

and

$$\hat{B}_2 = \left\{ \begin{pmatrix} -\mathrm{pp}'d_+ & -\frac{\mathrm{p}}{m_\Delta}(\varepsilon_\pi(\varepsilon_\pi+m_\Delta c)-b(\theta'+\varepsilon_\pi^2)) \\ \frac{\mathrm{p}'}{m_\Delta}(\varepsilon_\pi(\varepsilon_\pi+m_\Delta c)-b(\theta+\varepsilon_\pi^2)) & -\varepsilon_\pi\left(\frac{b(\theta+\theta')}{m_\Delta}+\frac{2\varepsilon_\pi^2 x_\Delta}{m_\Delta}+\varepsilon_\pi d_-\right) \end{pmatrix} \right.$$
$$\left. + \mathrm{pp}'x \begin{pmatrix} 0 & \frac{\mathrm{p}}{m_\Delta} \\ -\frac{\mathrm{p}'}{m_\Delta} & 2\left(d_- - \frac{\varepsilon_\pi}{m_\Delta}\right) \end{pmatrix} \right\}. \quad \text{(A18)}$$

In the above, $d_\pm$ is as defined in Eq. (A13) and we have used

$$\theta = \varepsilon_\pi\sqrt{s} - 2\varepsilon_\pi^2 + \mathrm{p}^2; \qquad \theta' = \varepsilon_\pi\sqrt{s} - 2\varepsilon_\pi^2 + \mathrm{p}'^2, \quad \text{(A19)}$$

$$a = \frac{\theta+\theta'+m_\Delta^2}{m_\Delta}, \quad \text{(A20)}$$

$$b = 1 + x_\Delta, \quad \text{(A21)}$$

$$c = 1 + 2x_\Delta, \quad \text{(A22)}$$

and

$$\zeta = \sqrt{s} - 2\varepsilon_\pi = \varepsilon_N - \varepsilon_\pi. \quad \text{(A23)}$$

The rho exchange contribution is

$$\hat{V}_\rho^{I\pm JT}(\mathrm{p},\mathrm{p}';s) = 6\pi g_\rho^2(-1)^{T+\frac{1}{2}} \begin{Bmatrix} \frac{1}{2} & \frac{1}{2} & 1 \\ 1 & 1 & T \end{Bmatrix} f_N(p_N^2) f_\pi(p_\pi^2) f_N(p_N'^2) f_\pi(p_\pi'^2) \int_{-1}^{+1} dx \frac{f_\rho^2(t)}{t-m_\rho^2}$$

$$\times \left[\begin{pmatrix} -2\varepsilon_\pi + \frac{\kappa_\rho \mathrm{p}\mathrm{p}'x}{m_N} & -\mathrm{p}'\left(1 - \frac{\kappa_\rho \varepsilon_\pi}{m_N}\right) \\ \mathrm{p}\left(1 - \frac{\kappa_\rho \varepsilon_\pi}{m_N}\right) & -\frac{\kappa_\rho \mathrm{p}\mathrm{p}'}{m_N} \end{pmatrix} P_l(x) \right.$$

$$\left. + \begin{pmatrix} -\frac{\kappa_\rho \mathrm{p}\mathrm{p}'}{m_N} & -\mathrm{p}\left(1 + \frac{\kappa_\rho \varepsilon_\pi}{m_N}\right) \\ \mathrm{p}'\left(1 + \frac{\kappa_\rho \varepsilon_\pi}{m_N}\right) & 2\varepsilon_\pi + \frac{\kappa_\rho \mathrm{p}\mathrm{p}'x}{m_N} \end{pmatrix} P_{l\mp1}(x) \right]. \tag{A24}$$

Finally, the sigma exchange is given by

$$\begin{aligned} \widehat{V}_\sigma^{l\pm JT}(\mathrm{p},\mathrm{p}';s) &= 2\pi \frac{g_{\sigma NN} g_{\sigma\pi\pi}}{2m_\pi} f_N(p_N^2) f_\pi(p_\pi^2) f_N(p_N'^2) f_\pi(p_\pi'^2) \int_{-1}^{+1} dx \frac{f_\sigma^2(t)}{t - m_\sigma^2} \\ &\times (\varepsilon_\pi^2 - \mathrm{p}\mathrm{p}'x) \begin{pmatrix} P_l(x) & 0 \\ 0 & P_{l\mp1}(x) \end{pmatrix}. \end{aligned} \tag{A25}$$

References

[1] K. Erkelenz, Phys. Rep. **13** (1974) 191.

[2] G.E. Brown and A.D. Jackson, The nucleon-nucleon interaction (North-Holland, Amsterdam, 1976).

[3] E.D. Cooper, B.C. Clark, R. Kozack, S.Shim, S, Hama, J.I. Johansson, H.S. Sherif, R.L. Mercer, and B.D. Serot, Phys. Rev. **C36** (1987) 2170.

[4] K. Stricker, H. McManus and J.A. Carr, Phys. Rev. **C19** (1979) 929.
K. Stricker, J.A. Carr and H. McManus, Phys. Rev. **C22** (1980) 2043.
J.A. Carr, H. McManus and K. Stricker-Bauer, Phys. Rev. **C25** (1982) 952.

[5] E.R. Siciliano, M.D. Cooper, M.B. Johnson, and M.J. Leitch, Phys. Rev. **C34** (1986) 267.

[6] E.D. Cooper, K.H. Hicks and B.K. Jennings, Nucl. Phys. **A470** (1987) 523.

[7] E.D. Cooper and B.K. Jennings, Nucl. Phys. **A483** (1988) 601.

[8] R. Blankenbecler and R. Sugar, Phys. Rev. **142** (1966) 1051.

[9] E.D. Cooper and B.K. Jennings, Nucl. Phys. **A500** (1989) 553.

[10] E.D. Cooper, B.K. Jennings, P.A.M. Guichon, and A.W. Thomas, Nucl. Phys. **A469** (1987) 717.

[11] G. Höhler, F. Kaiser, R. Koch and E. Pietarinen, Handbook of pion-nucleon scattering (Fachinformationszentrum, Karlsruhe, 1979).

[12] H.W. Crater and P. Van Alstine, Ann. of Phys. **148** (1983) 57.

[13] B.C. Pearce, in preparation.

[14] B.J. Read, Nucl. Phys. **B52** (1973) 565.

[15] A.W. Thomas, Adv. in Nucl. Phys. **13** (1984) 1.

[16] R. Machleidt, K. Holinde, and Ch. Elster, Phys. Rep. **149** (1987) 1.

[17] B.C. Pearce and I.R. Afnan, Phys. Rev. **C34** (1986) 991.

[18] G. Höhler and E. Pietarinen, Nucl. Phys. **B95** (1975) 210.

[19] B.C. Pearce and I.R. Afnan, Phys. Rev. **C40** (1989) 220.

[20] R. Koch and E. Pietarinen, Nucl. Phys. **A336** (1980) 331.

[21] O. Dumbrajs, R. Koch, H. Pilkuhn, G.C. Oades, H. Behrens, J.J. De Swart, and P. Kroll, Nucl. Phys. **B216** (1983) 277.

[22] R.D. Peccei, Phys. Rev. **176** (1968) 1812.

[23] L.M. Nath, B. Etemadi and J.D. Kimel, Phys. Rev. **D3** (1971) 2153.

[24] M.G. Olsson and E.T. Osypowski, Nucl. Phys. **B101** (1975) 136.

Tables

Table I. The parameters obtained by fitting to the Karlsruhe[11] phase shifts using the indicated propagators. Parameters with energy dimensions (m's and Λ's) are in MeV. Note that the K-matrix is insensitive to Λ_π.

Parameter	Smooth	BbS	K-matrix
$g^2_{\pi NN}/4\pi$	14.3	14.3	14.3
$g^2_{0\pi NN}/4\pi$	4.4088	6.4629	14.3
$g^2_{\pi N\Delta}/4\pi$	0.36	0.36	0.36
$g^2_{0\pi N\Delta}/4\pi$	0.17462	0.16764	0.36
$g^2_\rho/4\pi$	3.1349	2.9009	3.0326
κ_ρ	2.2543	1.4366	3.1597
$g_{\sigma NN}g_{\sigma\pi\pi}/4\pi$	143.60	227.72	210.95
x_Δ	−0.12391	−0.40766	−0.31130
m_{0N}	1093.2	1058.8	938.9
$m_{0\Delta}$	1427.7	1403.8	1232.0
m_σ	654.30	662.41	626.15
Λ_π	700.00	700.00	-
Λ_N	1116.6	1384.2	1333.9
Λ_Δ	1035.1	1389.9	1500.0
Λ_ρ	1214.3	1544.9	1402.6
Λ_σ	511.54	500.38	508.09

Table II. The scattering lengths and volumes obtained for the three fits presented in fig. 4 and table 1. Units are $m_\pi^{-(2l+1)}$.

Partial wave	Smooth	BbS	K-matrix	ref. [20]
S_{11}	0.150	0.151	0.172	0.173
S_{31}	−0.082	−0.092	−0.054	−0.101
P_{11}	−0.069	−0.072	−0.108	−0.081
P_{13}	−0.043	−0.040	−0.050	−0.030
P_{31}	−0.050	−0.048	−0.063	−0.045
P_{33}	0.244	0.230	0.200	0.214

Table III. A comparison of the coupling constant parameters from the fit with the smooth propagator with the values used by various other authors.

Parameter	Smooth	From other sources	Reference
$g^2_{\pi NN}/4\pi$	14.3	14.28	[20]
		14.4	[16]
$g^2_{0\pi NN}/4\pi$	4.4088	–	
$g^2_{\pi N\Delta}/4\pi$	0.36	0.35	[20] and [21]
		0.36	[16]
$g^2_{0\pi N\Delta}/4\pi$	0.17462	–	
$g^2_\rho/4\pi$	3.1349	3.36	[16]
	(2.2745)[a]	2.2	[18]
		3.54	[22]
κ_ρ	2.2543	6.6	[18]
		3.7	[22]
$g_{\sigma NN}g_{\sigma\pi\pi}/4\pi$	143.60	–	
x_Δ	−0.12391	−1	[23]
		−0.25	[22]
		−0.05	[24]

[a]This is the effective coupling constant at $t = 0$.

Table IV. Bare parameters used for the comparison in fig. 3.

Propagator	$g^2_{0\pi NN}/4\pi$	m_{0N} (MeV)	$g^2_{0\pi N\Delta}/4\pi$	$m_{0\Delta}$ (MeV)
Smooth	4.4088	1093.2	0.17462	1427.7
BbS	10.945	1093.1	0.23150	1419.8
K-matrix	14.3	938.9	0.36	1232

Figure Captions

1. The six diagrams included in the driving term.

2. (a) A comparison of the momentum dependence of our πNN form factor at $\sqrt{s} = m_N$ (solid curve) with the cloudy bag model using $R = 1.0$ fm (dashed curve) and the Bonn potential[16] (dash-dotted curve). (b) Our πNN form factor with $\sqrt{s} = m_N$ (solid curve), $\sqrt{s} = m_N + m_\pi$ (dashed curve) and $\sqrt{s} =$ 1400 MeV (dash-dotted curve).

3. A comparison of results using the same parameter set with the smooth propagator (solid curve), the Blankenbecler-Sugar propagator (dashed curve), and the K-matrix (dash-dotted curve).

4. A comparison of the results obtained by refitting the parameters to the data using the smooth (solid curve), the Blankenbecler-sugar (dashed curve), and the K-matrix (dash-dotted curve) propagators.

5. The contributions made by the various diagrams of fig. 1 to the Born term in each partial wave. The total and pole curves are omitted for the P_{11} and P_{33} channels since the energy region considered encompasses the poles.

6. (a) The S^+ and S^- scattering lengths as a function of pion mass for the fit using the smooth propagator. (b) The same for the Blankenbecler-Sugar propagator.

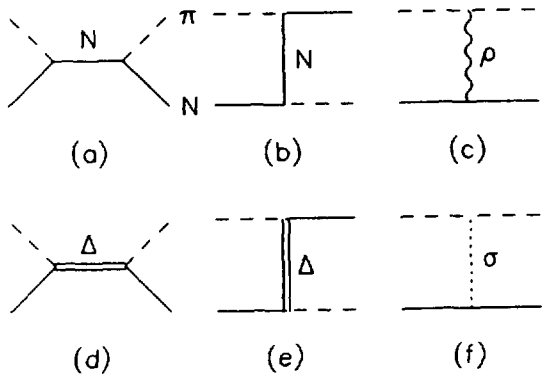

Fig. 1

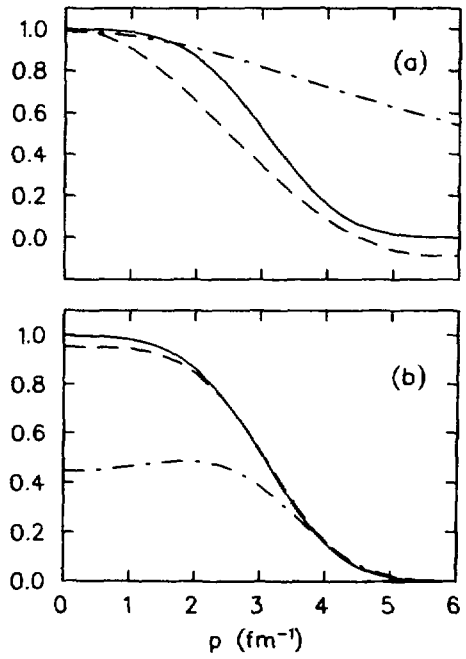

Fig. 2

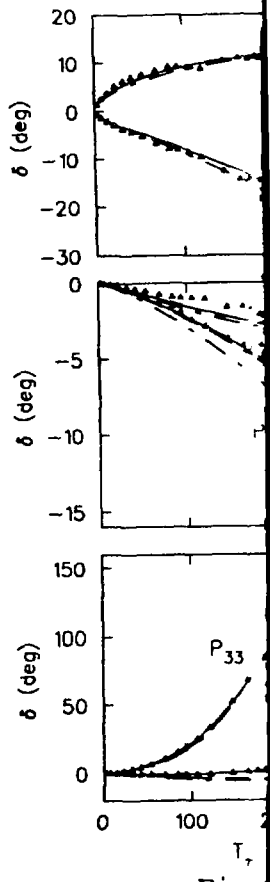

Fig

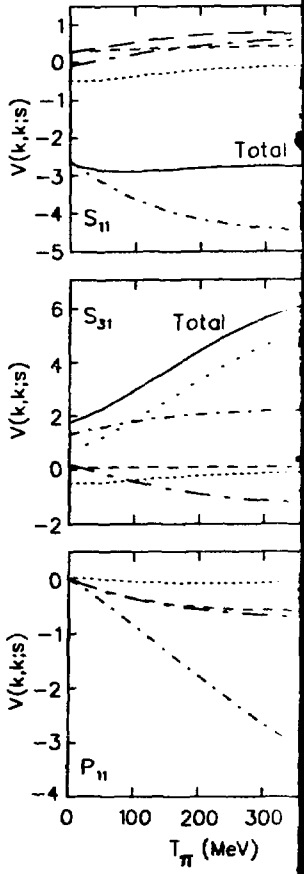

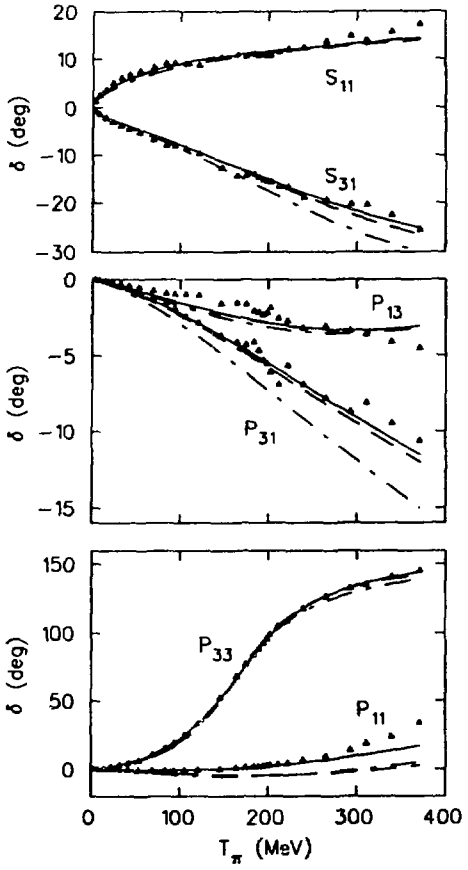

Fig. 3

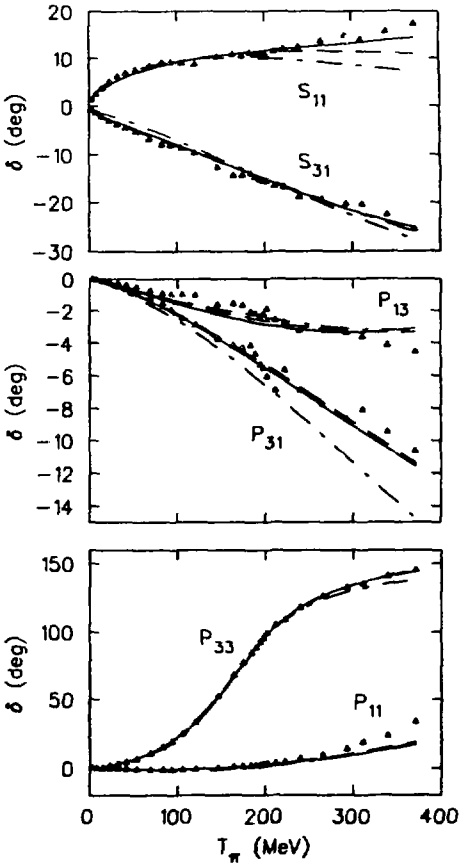

Fig. 4

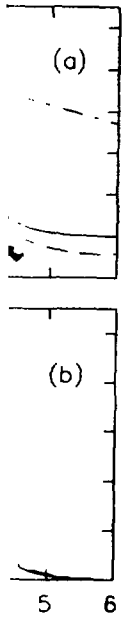

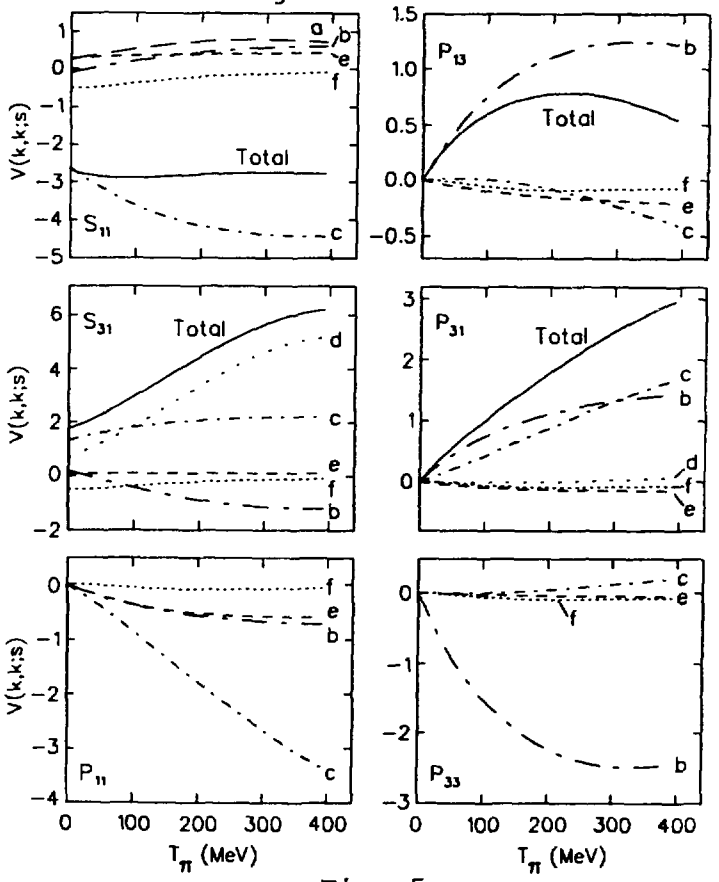

Fig. 5

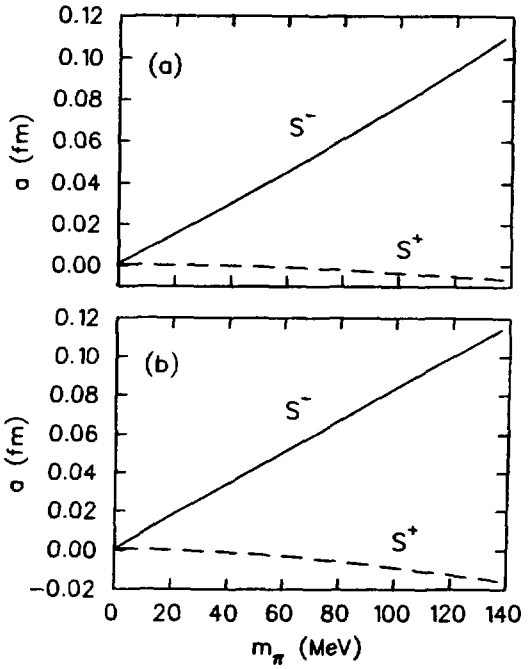

Fig. 6